International Journal of Heat and Mass Transfer 54 (2011) 5444–5458

Contents lists available at SciVerse ScienceDirect

International Journal of Heat and Mass Transfer

journal homepage: www.elsevier.com/locate/ijhmt

Heat transport from a bluff body near a moving wall at *Re* = 100

S. Dhinakaran *

Departamento de Engenharia Química, Faculdade de Engenharia da Universidade do Porto, Rua do Doutor Roberto Frias, 4200 465 Porto, Portugal

ARTICLE INFO

Article history:
Received 28 January 2011
Accepted 25 July 2011
Available online 24 August 2011

Keywords:
Square cylinder
Vortex shedding suppression
Moving wall
Forced convection heat transfer

ABSTRACT

Numerical simulations are performed for the flow and heat transfer from a stationary 2D square cylinder placed near a moving wall at Reynolds number 100 and cylinder-to-wall gap ratios in the range $0.1 \leqslant G/D \leqslant 4$. The governing equations are solved using a finite volume method. Flow and thermal field resemble that of isolated case when the cylinder is far away from the moving wall. When $G/D < 1$, the twin vortex shedding pattern is transformed into single row of negative vortices and eventually the flow becomes steady when $G/D < 0.3$. Lift ($\overline{C}_L$) and drag coefficient ($\overline{C}_D$) of the cylinder are higher compared to that of an isolated cylinder. Strouhal number (St) of the cylinder increases with decrease in gap ratio from 4 to 1. With a further decrease in gap ratio, St reduces drastically before vanishing at $G/D = 0.3$ as a consequence of vortex shedding suppression. In general, the heat transfer rates are higher than the case of an isolated cylinder. The mean Nusselt number (Nu_M) increases with decrement in gap ratio. However, the trend is not the same. Nu_M increases gradually when G/D is varied from 4 to 0.5, while it suddenly decreases with decrement in G/D from 0.5 to 0.3 and again rises sharply for $G/D \leqslant 0.2$. Results indicate that an enhancement of 27.45% in mean Nusselt number can be achieved, compared to the isolated case, by placing the cylinder at $G/D = 0.1$.

1. Introduction

When a uniform fluid stream flows past a stationary square cylinder the flow remains attached for $Re \leqslant 2$. When $Re > 2$, two symmetric recirculating eddies are formed behind the cylinder. These eddies remain symmetric and keep increasing in size up to $Re = 40$. For $Re > 40$, flow becomes unsteady and the negative and positive shear layers formed on the top and bottom surface of the cylinder, respectively, roll-up giving rise to two rows of alternate shedding of vortices called the Von Karman vortex street. If the cylinder is maintained at a temperature higher than the ambient, the shed vortices from the cylinder tends to enhance heat transfer rates by carrying the heat along with them. The amount of heat transported from the cylinder to the ambient fluid stream depends mainly on the Reynolds number of the flow. With an increase in Re the heat transfer rates from the cylinder increases. This phenomenon plays an essential role in the design of heat exchangers, vortex shedding flow meters, magnetic disc-storage devices, power cables and in cooling of electronic components [1]. Due to this reason unsteady flow and heat transfer from isolated square cylinders have been the subject of numerous scientific investigations in the past [2,3].

However, based on early experimental and numerical studies, it has been established that the flow pattern behind the square/circular cylinder is greatly altered when a plane wall, either stationary or in motion, is brought in proximity. The modification in flow pattern depends on how close the moving or stationary plane wall is brought near the cylinder and the flow Reynolds number. Since the flow pattern changes with the introduction of a wall, heat transport, too, varies that depends on two parameters: Reynolds number and gap ratio. When a cylinder is brought near a stationary or moving wall, for the conditions of unsteady flow, vortex shedding is suppressed below a certain gap ratio called the critical gap ratio. The gap ratio is a non-dimensional parameter which is the ratio of gap distance between the cylinders' bottom surface and plane wall, G, and the cylinder diameter, D and is denoted by G/D.

As stated earlier, the flow pattern behind a bluff body is greatly altered in the presence of a stationary wall compared to the isolated case. In an early experimental study on vortex shedding from a circular cylinder in a towing water tank, Taneda [4], observed a single row of vortices, rather than two-rows of alternately shed vortices, when the cylinder was towed very close to the wall. For the case of a circular cylinder, Bearman and Zdravkovich [5] established that a gap ratio of 0.3 is enough to suppress the vortex shedding phenomenon. In a flow visualization study, Price et al. [6] showed that vortex shedding is suppressed for $G/D \leqslant 0.125$. Bailey et al. [7] measured the pressure and velocity field near a square cylinder in proximity to a solid wall at $Re = 19{,}000$. Their study

* Tel.: +351 225 08 1779; fax: +351 225 081 404.
E-mail address: ssdhinakar@gmail.com

0017-9310/$ - see front matter © 2011 Elsevier Ltd. All rights reserved.
doi:10.1016/j.ijheatmasstransfer.2011.07.046

Nomenclature

AB	front face of the cylinder
BC	bottom face of the cylinder
CD	rear face of the cylinder
DA	top face of the cylinder
D	height of the square cylinder
C_L	lift coefficient, $\frac{F_L}{\frac{1}{2}\rho U_\infty^2 D}$
C_{LP}, C_{LV}	lift coefficient due to pressure and viscous forces
C_D	drag coefficient, $\frac{F_D}{\frac{1}{2}\rho U_\infty^2 D}$
C_{DP}, C_{DV}	drag coefficient due to pressure and viscous forces
C_p	specific heat capacity
C_P	pressure coefficient, $\frac{p-p_\infty}{\frac{1}{2}\rho U_\infty^2}$
f	frequency of vortex shedding, $\frac{1}{T}$
G	dimensional distance between the bottom surface of cylinder and the plane wall
G/D	gap ratio or Non-dimensional distance between the bottom surface of cylinder and the plane wall
k	thermal conductivity
L_{us}	length of upstream boundary from the front face of the cylinder
L_{ds}	length of downstream boundary from the rear face of the cylinder
L_h	length of top boundary from the top face of the cylinder
Nu	local Nusselt number on a face of the cylinder, $-\left(\frac{\partial \Theta}{\partial y}\right)_{\text{surface}}$
$\overline{\text{Nu}}$	average Nusselt number on any face of the cylinder, $\int_0^1 \left(-\frac{\partial \Theta}{\partial n}\right) dl$
Nu_M	mean Nusselt number of the cylinder, $\frac{1}{4}\sum_{AB}\overline{\text{Nu}}_{f,r,t,b}$
p	non-dimensional pressure, $\frac{p}{\rho U_\infty^2}$
P	dimensional pressure
Pr	Prandtl number, $\frac{\nu}{\alpha}$
Re	Reynolds number, $\frac{UD}{\nu}$
St	Strouhal number, $\frac{fD}{U_\infty}$
t	dimensional time
T	period of vortex shedding
U_c	convective velocity
u, U	dimensional and non-dimensional x-component of velocity, respectively
v, V	dimensional and non-dimensional y-component of velocity, respectively
x, y	horizontal and vertical coordinate

Greek

ϕ	dependent variable, U, V or Θ
μ	viscosity of the fluid
τ	non-dimensional time
ρ	fluid density
θ	dimensional temperature
Θ	dimensionless temperature, $\frac{(\theta-\theta_\infty)}{(\theta_H-\theta_\infty)}$

Subscript

∞	far field value
H	high value
f	front face
r	rear face
t	top face
b	bottom face
M	mean value
us	upstream
ds	downstream

showed that vortex shedding is suppressed for $G/D < 0.4$. While studying the shear flow past a square body near a stationary plane wall, Bhattacharyya and Maiti [8] found that vortex shedding is suppressed even at $Re = 100$ for $G/D = 0.5$. More recently, Mahir [9] made a 3D study of the flow past a square cylinder placed near a moving wall for gap ratios in the range 0.2 to 4 and for Reynolds numbers 175, 185 and 250. These studies clearly shows that a stationary plane wall modifies the flow pattern when a bluff body is placed in proximity and the unsteady flow turns steady below a critical gap ratio with an alteration in flow parameters such as drag and lift coefficients, Strouhal number (St), pressure distribution etc.

When a hot bluff body is brought in proximity to a plane stationary wall, the amount of heat transfered from the body depends on various factors such as the Reynolds number, gap ratio, heating conditions (constant temperature or constant heat flux) and the type of heat transfer (forced, mixed or natural convection). Yang et al. [10] analyzed the heat transfer from a circular cylinder under the effect of a plane solid wall for forced and mixed convection regime. They found an accelerating effect with increase in Richardson number while the presence of plane wall showed an decelerating effect on the flow around the cylinder. The heat transfer rate and drag force increased with increasing G/D and Grashoff number. Shuja et al. [11] investigated the heat transfer characteristics of rectangular cylinder with ground effect for gap ratios in the range $1.3 \leqslant G/D \leqslant 8$. They examined the influence of St on the variation of Stanton number of the cylinder. The shedding frequency increased as gap height reduced and with further reduction in gap height resulted in diminishing of vortex shedding. Bhattacharyya et al. [12] studied the mixed convection heat transfer from a square cylinder, in shear flow, at a gap ratio of 0.5 near a stationary plane wall. Their results indicated that vortex shedding is delayed when the heat input to the cylinder is increased or in other words when the Richardson number, Ri, is increased. Heat transfer rates increased with increasing values of Ri at $Re = 125$. Whereas, at higher Re, the heat transfer rates showed a minimal change with increase in Ri. Chakraborthy and Brahma [13] made an experimental investigation on heat transfer due the effect of placing a square prism from a plane wall at various gap ratios and angle of attack. The mean Nusselt number of the prism reduced with decrease in gap ratio. Heat transfer from a circular cylinder placed near a plane stationary wall at $20 \leqslant Re \leqslant 200$ for $0.1 \leqslant G/D \leqslant 2$ was made by Singha et al. [14]. Vortex shedding was observed from one side of the cylinder and at the other side a strong jet action of the fluid through the gap between the cylinder and the wall was observed. The mean Nusselt number increased with increase in gap ratio from 0.1 up to a critical gap ratio that was dependent on the flow Reynolds number. Below a critical gap ratio, the Nusselt number decreased with an increase in gap-ratio before asymptotically reaching the Nusselt number of the isolated case. However, these studies concentrated on flow and heat transfer from square/cylindrical bluff bodies near a stationary plane wall.

Looking into these studies, it is quite clear that a bluff body brought in proximity of a plane stationary wall brings about a change in flow pattern and thus the heat transfer. Analysis of flow and heat transfer from bluff bodies near a moving wall is important since the flow pattern gets altered resulting in a change in thermal pattern and thus the heat transfer which is much different from the stationary wall case. Flow past moving vehicles near a plane road, ships and submarines near a plane wall are all akin to flow past a square cylinder near a plane-moving wall. In contrast to a cylinder in proximity of a stationary wall, where a boundary layer is

formed, the case of a cylinder near a moving wall is entirely different as no such boundary layer develops on the wall. Besides, this is also of academic interest similar to the case of flow and heat transfer from bluff bodies near a stationary wall. Moreover, the critical gap ratio at which vortex shedding ceases may also differ from the stationary wall case.

1.1. Previous works

Though several articles are available in the literature concerning the flow past a square/circular bluff body near a stationary plane wall, works on the same case but near moving wall is scant in the literature. In this context, Arnal et al. [15] studied the flow around a square bluff body in direct contact with a sliding wall. The flow around a half-cylinder in proximity to a plane moving wall has been analyzed by Kumaraswamy and Barlow [16]. They did RANS simulations at $Re = 4.68 \times 10^5$ for ∞ (isolated) $\leqslant G/D \leqslant$ 0.167 to predict the flow features, lift and drag coefficient and *St*. Their finding indicated an increase in lift coefficient with decrease in gap ratio. The *St* of the cylinder near the moving wall did not show any significant variation with gap ratio. Bhattacharyya and Maiti [17] numerically investigated the flow past a square cylinder near a moving wall for gap ratios 0.5, 0.25 and 0.1 and for $200 \leqslant Re \leqslant 1000$. In their study, vortex shedding was observed even at $G/D = 0.1$ at higher Reynolds numbers. The vortex shedding frequency reduced with reduction in *G*/*D*. The variation in drag coefficient with decrease in gap ratios, from 0.5 to 0.1, was small for those Reynolds numbers. The cylinder experienced a negative lift for $Re > 400$ at $G/D = 0.5$ and 0.25. Huang and Sung [18] studied the unsteady flow past a circular cylinder near a moving plane wall for Reynolds numbers in the range $200 \leqslant Re \leqslant 600$ and gap ratios (*G*/*D*) from 0.6 to 0.1. The mean drag coefficient increased when the gap ratio is decreased up to a critical value. Below the critical value, it started to decrease with a further decrease in gap ratio. But the lift coefficient increased with a decrease in gap ratio. When the gap ratio is reduced from $G/D = \infty$ to 0.6, *St* was found to increase. When *G*/*D* was varied from 0.6 up to the critical gap ratio, *St* started to decrease rapidly. With a further decrease in gap ratio up to 0.1, the decrease in *St* was gradual. Air flow in the gap between a car underbody and a moving ground was studied by Jones and Smith [19] for $1 \leqslant Re \leqslant 10^6$ for different underbody shapes. These studies were concerned with the 'fluid flow' aspects past a bluff body near a moving wall.

Concerning heat transfer from a bluff body near a moving wall, the works of Yoon et al. [20,21] are the only investigations available in the open literature. However, their investigation was focussed on a circular cylinder rather than a square cylinder. Yoon et al. [20] presented the flow and thermal field in forced convection around a circular cylinder near a plane moving wall at $Re = 100$, 140 and 180. The flow field showed two rows of vortices being shed from the cylinder at $G/D = 4$. With decreasing the gap ratio, at $Re = 100$, the two-row vortex structure was transformed into single-row vortex structure at $G/D = 0.5$ and the flow attained steady state at $G/D \leqslant 0.2$. For $Re > 100$ the single-row vortex structure appeared even at $G/D = 0.2$ and 0.1. *St* of the cylinder increased with decreasing gap ratio up to 0.5, and decreased for $G/D < 0.5$. The lift coefficient increased with increase in *G*/*D*. Yoon et al. [21] extended the earlier work of Yoon et al. [20] for the same gap ratios but for a wide range of Reynolds numbers i.e., $60 \leqslant Re \leqslant 200$. They demonstrated the dependence of critical gap ratio on Reynolds number.

1.2. Objective of this study

From the above discussion it is clear that there is no detailed analysis available, in the open literature, on how the flow pattern behind an isolated cylinder varies when it is gradually brought in proximity, from far field, to a plane moving wall. Besides, a study on the forced convection heat transfer for this configuration is also not available in the archival literature. Works on the same topic with a different geometry, i.e., a circular cylinder, do exist [20,21] in the literature. Therefore, this study aims to fill this gap. A systematic study has been made to analyze the flow and also the thermal field around a square cylinder in the vicinity of a plane moving wall for gap ratios in the range $4 \leqslant G/D \leqslant 0.1$ and also for the isolated case. The variation of parameters such as lift and drag coefficients, Strouhal number, pressure distribution and Nusselt number of the cylinder with gap ratio are presented. The flow and thermal pattern in the vicinity of the cylinder and the plane moving wall are presented with the help of contours of vorticity and isotherms. Only a particular Reynolds number of 100 is chosen for the analysis. At this *Re*, the flow past an isolated cylinder shows an unsteady behaviour with periodic vortex shedding. Moreover, at this value of *Re* the flow is laminar and two-dimensional.

The remaining of the paper is organized as follows: The mathematical formulation that includes the problem description, governing equations, boundary conditions and the definition of the parameters used in this study are presented in Section 2 while Section 3 presents the numerical method used, size of computational domain, grid structure, grid dependence study and the validation of the code used for the calculations in this study. The results of the study are discussed in Section 4. Important conclusions from this study are presented in the last section (Section 5).

2. Mathematical formulation

2.1. Problem description

Consider a 2D square cylinder of height, *D*, placed at a distance of '*G*' above a plane wall as illustrated in Fig. 1(*a*). The cylinder is stationary and is maintained a constant temperature, θ_H, higher than the ambient whose temperature is θ_∞. The cylinder is exchanging heat with the surrounding fluid stream which is flowing with a uniform velocity U_∞. The plane wall is moving from left to right in the positive *x*-direction at a uniform velocity U_∞ (which is same as the far field velocity). Artificial boundaries are placed at sufficient distance far away from the cylinder in order to make the problem computationally feasible.

2.2. Governing equations

The equations governing the 2D, laminar, incompressible flow and heat transfer from a square cylinder are the continuity, Navier–Stokes and energy equation in the dimensional form and is given as:

Continuity equation:

$$\frac{\partial u}{\partial x} + \frac{\partial v}{\partial y} = 0 \tag{1}$$

Momentum equations:

$$\rho\left(\frac{\partial u}{\partial t} + u\frac{\partial u}{\partial x} + v\frac{\partial u}{\partial y}\right) = -\frac{\partial p}{\partial x} + \mu\left(\frac{\partial^2 u}{\partial x^2} + \frac{\partial^2 u}{\partial y^2}\right) \tag{2}$$

$$\rho\left(\frac{\partial v}{\partial t} + u\frac{\partial v}{\partial x} + v\frac{\partial v}{\partial y}\right) = -\frac{\partial p}{\partial y} + \mu\left(\frac{\partial^2 v}{\partial x^2} + \frac{\partial^2 v}{\partial y^2}\right) \tag{3}$$

Energy equation:

$$\rho C_p\frac{\partial \theta}{\partial t} + \rho C_p\left(u\frac{\partial \theta}{\partial x} + v\frac{\partial \theta}{\partial y}\right) = k\left(\frac{\partial^2 \theta}{\partial x^2} + \frac{\partial^2 \theta}{\partial y^2}\right) \tag{4}$$

The following characterisitic scales are introduced to non-dimensionalize the above governing equations:

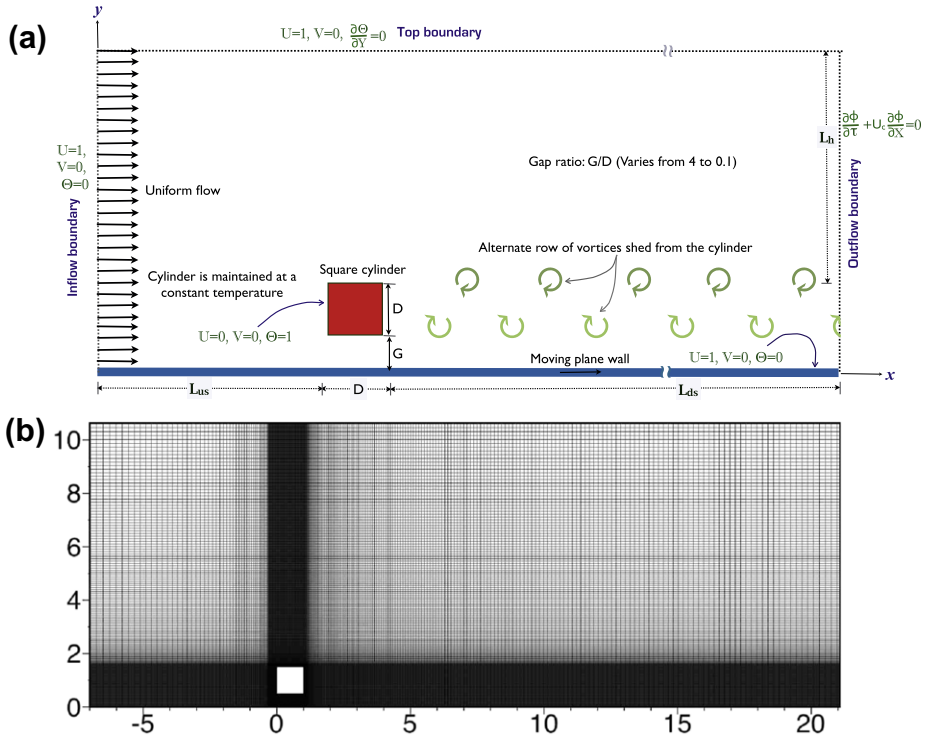

Fig. 1. (a) Sketch of the flow configuration for the uniform flow of air past a heated square cylinder placed near a plane moving wall; (b) mesh distribution in the vicinity of the plane wall and the cylinder at $G/D = 0.5$.

$$X = \frac{x}{D}, \quad Y = \frac{y}{D}, \quad \tau = \frac{tU_\infty}{D}, \quad P = \frac{p}{\rho U_\infty^2},$$
$$U = \frac{u}{U_\infty}, \quad V = \frac{u}{U_\infty}, \quad \Theta = \frac{(\theta - \theta_\infty)}{(\theta_H - \theta_\infty)}.$$

Assuming negligible viscous dissipation, the dimensionless form of the governing equations for the incompressible flow of a constant viscosity fluid past a square cylinder is presented as follows:

Continuity equation:

$$\frac{\partial U}{\partial X} + \frac{\partial V}{\partial Y} = 0 \tag{5}$$

Momentum equations:

$$\frac{\partial U}{\partial \tau} + \left(U\frac{\partial U}{\partial X} + V\frac{\partial U}{\partial Y}\right) = -\frac{\partial P}{\partial X} + \frac{1}{Re}\left(\frac{\partial^2 U}{\partial X^2} + \frac{\partial^2 U}{\partial Y^2}\right) \tag{6}$$

$$\frac{\partial V}{\partial \tau} + \left(U\frac{\partial V}{\partial X} + V\frac{\partial V}{\partial Y}\right) = -\frac{\partial P}{\partial Y} + \frac{1}{Re}\left(\frac{\partial^2 V}{\partial X^2} + \frac{\partial^2 V}{\partial Y^2}\right) \tag{7}$$

Energy equation:

$$\frac{\partial \Theta}{\partial \tau} + \left(U\frac{\partial \Theta}{\partial X} + V\frac{\partial \Theta}{\partial Y}\right) = \frac{1}{Re.Pr}\left(\frac{\partial^2 \Theta}{\partial X^2} + \frac{\partial^2 \Theta}{\partial Y^2}\right) \tag{8}$$

The dimensionless variables are defined as: $Re = \rho U_\infty D/\mu$ is the Reynolds number, $Pr = \mu C_p/k$ is the Prandtl number.

2.3. Boundary conditions

Following are the conditions applied at various boundaries in order to solve the flow problem:

- *Inflow boundary (inlet)*: At the inflow boundary a uniform flow profile is assumed. i.e., $U = 1$, $V = 0$ and $\Theta = 0$.
- *Top and bottom boundaries*: $U = 1$, $V = 0$ and $\frac{\partial \Theta}{\partial Y} = 0$.
- *Outflow boundary (exit)*: The convective boundary condition has been used as it decreases the number of time step, and allows lower downstream length (L_{ds}) to be used [22], and is given by

$$\frac{\partial \phi}{\partial t} + U_c\frac{\partial \phi}{\partial X} = 0 \tag{9}$$

where U_c is the average non-dimensional streamwise velocity (equal to unity) and ϕ is the dependent variable U, V or Θ.
- *On the cylinder surface*: Non-slip conditions for the velocities and a constant temperature conditions are applied on the cylinder surface. i.e., $U = 0$, $V = 0$, $\Theta = 1$
- *On the plane wall*: $U = 1$, $V = 0$, $\Theta = 0$

2.4. Definitions of certain parameters

It is now useful to define some of the parameters used in this study.

2.4.1. Lift (C_L) and drag (C_D) coefficient

The lift and drag coefficient of the cylinder are calculated as

$$C_L = C_{LP} + C_{LV} = \frac{F_L}{\frac{1}{2}\rho U_\infty^2 D} \tag{10}$$

$$C_D = C_{DP} + C_{DV} = \frac{F_D}{\frac{1}{2}\rho U_\infty^2 D} \tag{11}$$

where, C_{LP} and C_{LV} represent the lift coefficient due to pressure and viscous force, respectively. Similarly, C_{DP} and C_{DV} represent the drag coefficient due to pressure and viscous force, respectively. F_L and F_D are the lift and drag forces acting on the cylinder. The lift and drag coefficients due to pressure and viscous forces can be obtained from the following expression:

$$C_{LP} = 2.0\int_0^1 (P_f - P_b)dY, \quad C_{LV} = \frac{2.0}{Re}\int_0^1 \left[\left(\frac{\partial U}{\partial Y}\right)_f + \left(\frac{\partial U}{\partial Y}\right)_r\right]dx$$

$$C_{DP} = 2.0\int_0^1 (P_f - P_r)dY, \quad C_{DV} = \frac{2.0}{Re}\int_0^1 \left[\left(\frac{\partial U}{\partial Y}\right)_b + \left(\frac{\partial U}{\partial Y}\right)_t\right]dx$$

with P representing the non-dimensional pressure acting on the surface of the cylinder. The subscripts f, r, t and b refer to front, rear, top and bottom surfaces of the cylinder, respectively. The mean values of the drag and lift coefficients are obtained by taking the average of their time histories.

2.4.2. Strouhal number

The dimensionless vortex shedding frequency of the cylinder is given by the Strouhal number (St) defined as

$$St = \frac{fD}{U_\infty} \tag{12}$$

where, f is the frequency of vortex shedding.

2.4.3. Pressure coefficient

The pressure coefficient (C_P) is defined by

$$C_P = \frac{p - p_\infty}{\frac{1}{2}\rho U_\infty^2} \tag{13}$$

where, p and p_∞ are the dimensional pressure on the cylinder surface and far field, respectively.

2.4.4. Nusselt number

Heat transfer from the cylinder to the flowing fluid is calculated from the local Nusselt number given by $\mathrm{Nu} = -\frac{\partial \Theta}{\partial n}$. Here, n is the direction normal to a cylinder surface. Average Nusselt number ($\overline{\mathrm{Nu}}$) at any face of the cylinder is obtained by integrating the local Nusselt number along that face. The average Nusselt number on the front (f), rear (r), top (t) and bottom (b) face of the cylinder is calculated as

$$\overline{\mathrm{Nu}}_f = -\int_A^B \mathrm{Nu}\ dy; \overline{\mathrm{Nu}}_t = -\int_D^A \mathrm{Nu}\ dx;$$

$$\overline{\mathrm{Nu}}_r = -\int_C^D \mathrm{Nu}\ dy \quad \text{and } \overline{\mathrm{Nu}}_b = -\int_B^C \mathrm{Nu}\ dx. \tag{14}$$

The total heat transfer rate from the cylinder is presented in terms of mean Nusselt number ($\mathrm{Nu_M}$). $\mathrm{Nu_M}$ is obtained as a mean value of the average Nusselt number on all the surfaces as shown below

$$\mathrm{Nu_M} = \frac{1}{4}\sum_{AB} \overline{\mathrm{Nu}}_{f,r,t,b}. \tag{15}$$

3. Numerical details

The governing equations Eqs. (5)–(8) are numerically solved using the SIMPLE algorithm [23]. These equations are discretized by integrating over square or rectangular control volumes. A staggered grid system is used in which the velocity components are stored at the midpoints of the cell while the scalar quantities such as pressure and temperature are stored at the center of the cell. A first order implicit scheme has been used to discretize the time derivatives while a third-order accurate scheme called QUICK (quadratic upwind interpolation for convective kinematics) of Leonard [24] has been used for discretizing the convective terms. The central difference scheme is used for the diffusion terms. The pressure link between continuity and momentum is achieved by transforming the continuity equation into a Poisson equation for pressure. The Poisson equation implements a pressure correction for a divergent velocity field. The resulting tridiagonal system of algebraic equations are solved through a block elimination method at each time step. Iterations are continued until a divergence-free velocity field is obtained. The solution is assumed to be converged when the divergence in each cell falls well below $\leqslant 10^{-8}$. Using the updated value of the velocity, Eq. (8) is solved to obtain Θ at each cell center.

3.1. Size of computational domain, grid structure, grid dependence study

The computational domain is rectangular. The inflow boundary and the top lateral boundary are placed sufficiently far away from the cylinder such that they do not influence the results. The inflow boundary lies at a distance $L_{us} = 10D$ from the front surface while the top later boundary lies at $L_h = 15D$ from the top surface of the cylinder. Initially, a downstream boundary length of $L_{ds} = 25D$ is chosen. The influence of L_{ds} on the mean drag coefficient and mean Nusselt number of the cylinder are tested for three more values of L_{ds}, namely $L_{ds} = 30D$, $35D$ and $45D$. As shown in Table 1, a value of $L_{ds} = 35D$ has been found to be the optimum value and has been used for all the cases used in this study.

The computational domain consists of a non-uniform mesh distribution. The grids are sufficiently fine near the cylinder surface and the moving wall, to capture the fine details of the flow, and coarse elsewhere. The grids are stretched in geometric progression. To test and assess the grid independent solutions, numerical experiments were performed for various grid sizes for each value of G/D used in this study. For the sake of brevity, the grid dependence tests made at $G/D = 0.5$ is only presented and discussed here.

The following four different size of mesh has been used to check the dependence of grid on the average drag coefficient ($\overline{C}_D$) and mean Nusselt number ($\overline{\mathrm{Nu}}_M$) of the cylinder at $G/D = 0.5$: 275×175 (Grid A), 550×350 (Grid B), 825×525 (Grid C) and 1100×700 (Grid D). The minimum distance of the first grid point from the moving wall and the cylinder surface is $\delta = 0.001$. The dependence of mesh size on $\overline{C}_D$ and Nu_M is presented in Table 1. Looking at Table 1, one can find that Mesh C and D produce grid independent results with the changes in $\overline{\mathrm{Nu}}$ occurring only at the third decimal place. A similar argument can be made for the downstream length at $L_{ds} = 35D$. The percentage difference in $\overline{C}_D$ and $\overline{\mathrm{Nu}}_M$ while using Mesh C and $L_{ds} = 35D$ is less than 1% when compared to Mesh D and $L_{ds} = 45D$. Hence Mesh C is chosen for further computation as it presents the best flow field with the least computational time. The grid resolution in the computational domain as well as near the walls are shown in Fig. 1(*b*).

3.2. Code validation

In order to validate the code used in the present study, quantities such as average drag coefficient ($\overline{C}_D$), Strouhal number (St) and mean Nusselt number (Nu_M) for the uniform flow past an isolated square cylinder were computed at $50 \leqslant Re \leqslant 200$ as depicted in Fig. 2(a)–(c). The numerical results for $\overline{C}_D$ obtained with the present code for the case of isolated cylinder is shown by a solid line while the results for the same case available in the literature are shown by symbols. The results of Sohankar et al. [22] is the lowest followed by those of Sharma and Eswaran [25]. Whereas, the corresponding values of Shimizu and Tanida (experimental data) [26] and Franke et al. [27] are higher than those of Sohankar et al. [22] and Sharma and Eswaran [25]. The present results lie well in between those results as seen in Fig. 2(*a*). In fact, the present results are in excellent agreement with those of Shimizu and Tanida [26].

Similarly, the present results for St [cf. Fig. 2(*b*)] is in good agreement with the results of Franke et al. [27], Sohankar et al. [28],

Table 1
Grid sensitivity and downstream length (L_{ds}) dependence test on average drag coefficient ($\overline{C}_D$) and mean Nusselt number (Nu_M) at gap ratio $G/D = 0.5$ for the flow past a square cylinder placed near a moving wall at $Re = 100$.

	Average drag coefficient ($\overline{C}_D$)				Mean Nusselt Number (Nu_M)			
Grids ($m \times n$)	$L_{ds} = 25D$	$30D$	$35D^*$	$45D$	$L_{ds} = 25D$	$30D$	$35D^*$	$45D$
275×175 (Grid A)	2.952	2.586	2.143	2.139	4.188	4.225	4.425	4.431
550×350 (Grid B)	2.658	2.226	2.104	2.099	4.016	4.310	4.358	4.363
825×525 (Grid C*)	2.251	2.153	2.097	2.095	3.915	4.220	4.233	4.236
1100×700 (Grid D)	2.249	2.153	2.096	2.095	3.915	4.219	4.233	4.234

* Mesh and Downstream length (L_{ds}) used in this study.

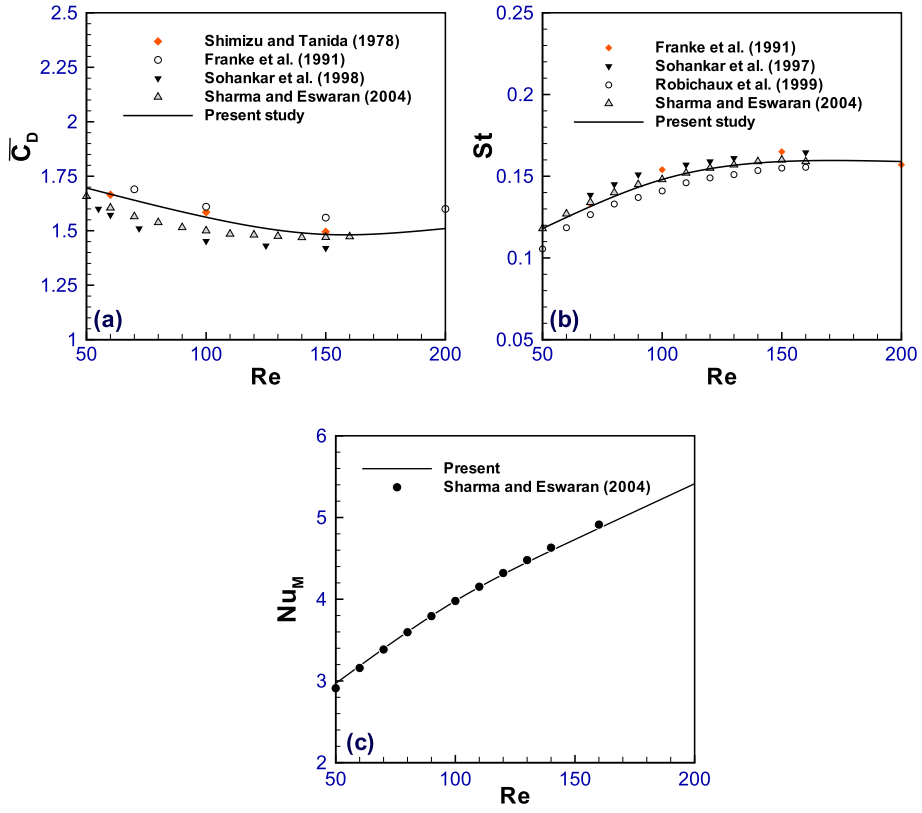

Fig. 2. Comparison of the computed (a) average drag coefficient ($\overline{C}_D$); (b) Strouhal number (St) and (c) mean Nusselt number (Nu_M) at Reynolds numbers $50 \leqslant Re \leqslant 200$ for the unconfined flow past a square cylinder with those available in the literature.

Robichaux et al. [29] and Sharma and Eswaran [25]. Finally, the computed results for the mean Nusselt number of an isolated cylinder is found to be in excellent agreement with those of Sharma and Eswaran [25] as seen in Fig. 2(*c*).

4. Results and Discussion

Forced convection heat transfer of air flow from a square cylinder placed near a plane moving wall has been considered in this study. A square cylinder of height, D, is placed at different heights (G) from the plane wall and the effect of cylinder-to-wall gap ratio (G/D) has been investigated numerically. The following are the parameters that affect the flow and thermal field given by.

- Reynolds number (Re): 100
- Gap ratio (G/D): 0.1–1 in steps of 0.1, 1.5, 2, 4 and ∞ (isolated case)
- Prandtl number (Pr): 0.71 (air)

4.1. Flow characteristics

4.1.1. Time evolution of lift coefficient and drag coefficient

The time evolution of lift coefficient (*dashed lines*) and drag coefficient (*solid lines*), calculated as per Eqs. (10) and (11), are presented in Fig. 3 at gap ratios, $G/D = 4$, 2, 1, 0.5, 0.4, 0.3 and 0.2. Observing this figure, one can find that, in general, C_L is oscillatory and oscillates periodically with time for $0.4 \leqslant G/D \leqslant 4$. At $G/D = 0.3$, the curve is weakly oscillating and at $G/D = 0.2$ it attains a steady state.

When the cylinder is isolated, the alternate shedding of negative and positive vortices results in a maximum and minimum value of lift coefficient during a vortex shedding cycle. The lift coefficient oscillates above and below zero with equal amplitude and thus the average lift coefficient is zero for the isolated square cylinder. For the case of square cylinder placed in proximity of a moving wall, at $G/D = 4$, the effect of moving wall is slightly felt by the cylinder. The lift coefficient profile is slightly shifted upwards, from the center (which is equal to zero in case

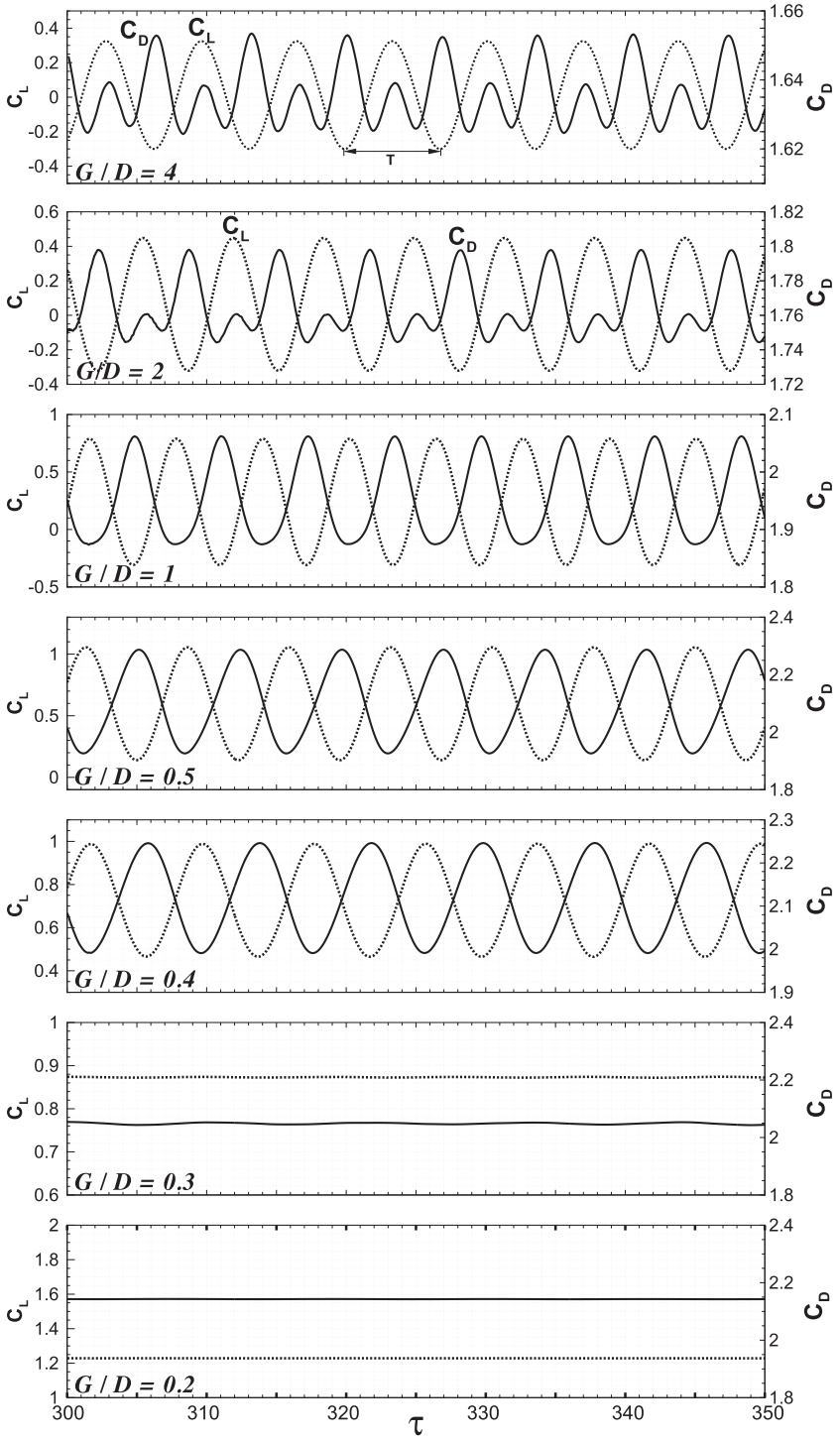

Fig. 3. Time evolution of drag coefficient (C_D, *solid line*) and lift coefficient (C_L, *dotted line*) at various gap ratios, G/D, for the flow past a square cylinder near a plane moving wall.

of an isolated square cylinder) resulting in a small positive value of C_L at $G/D = 4$. When the gap ratio is further decreased from $G/D = 4$ to $G/D = 1$, the lift coefficient starts to shift further upwards, from the center, and oscillates with more positive values. At $G/D \leqslant 0.5$, the lift coefficient completely attains positive values. At $G/D = 0.3$, the lift coefficient shows a quasi-steady profile as the flow attains a quasi-steady state. When $G/D < 0.3$, C_L is a straight line indicating that the flow has achieved a steady state and the vortex shedding is suppressed due to the moving wall.

The time evolution of drag coefficient shows a similar feature to that of an isolated square cylinder at $G/D = 4$ with two peaks during a period (T) of a vortex shedding cycle. At $G/D = 2$, the second peak starts to flatten and vanishes with decreasing G/D. For $0.4 \leqslant G/D \leqslant 1$, the C_D curve oscillates with the same frequency as that of the lift coefficient as observed in Fig. 3. While the drag

coefficient weakly oscillates at $G/D = 0.3$, it becomes steady at $G/D = 0.2$.

4.1.2. Instantaneous vorticity pattern

Contours of instantaneous vorticity that evolve from the cylinder in the presence of a moving wall are shown in Fig. 4(a) at $G/D = 4$, 2, 1, 0.5, 0.3, 0.2 and 1 at $Re = 100$. At $G/D = 4$ the flow is characterized by alternate negative and positive vortices being shed from the top and bottom surface of the cylinder, respectively. The two rows of alternately shed vortices almost resemble that of an isolated square cylinder in uniform flow. For brevity, the vorticity contours for the isolated case are not shown here. Along the moving plane wall, weak negative and positive vortices appear. When the cylinder is brought close to the moving wall at $G/D = 2$, the flow is again characterized by two-row vortex shedding. On the moving wall, negative and positive shear layers are formed that are stronger than the one formed at $G/D = 4$. When the cylinder is brought further closer to the moving wall at $G/D = 1$, the positive vortices shed from the cylinder starts to interact with the boundary layer negative vorticity of the moving wall. And now the wake is dominated mainly by the negative vortices shed from the top surface of the cylinder. The positive vortex that is shed from the bottom surface of the cylinder gets stretched when it interacts with the negative vorticity formed on the moving wall which delays the roll up process. At $G/D = 0.5$, the shear layers formed along the wall coalesce with the positive shear layer formed at the bottom surface of the cylinder and the vortices are stretched, resulting in a single row of vortices. This effect has also been observed in a similar study but with a circular cylinder near a plane moving wall by Huang and Sung [18] and Yoon et al. [20,21]. With further decrease in gap ratio, the shedding of single row of vortices cease and the flow becomes quasi-steady in nature (at $G/D = 0.3$). Below the critical gap ratio of $G/D = 0.3$ the flow attains a steady state with a steady wake formed behind the cylinder.

4.1.3. Vortex shedding during a cycle at G/D = 4, 1 and 0.4

Fig. 8(b) shows the instantaneous vorticity contours for the flow past a square cylinder near a moving wall at $G/D = 4$ at four instants during a vortex shedding cycle. The four instants denoted by A, B, C and D, in Fig. 8(a), correspond to $0 \times T$ (starting of the cycle), $\frac{1}{4} \times T$, $\frac{1}{2} \times T$ and $\frac{3}{4} \times T$, respectively. Where, T is the time period of the vortex shedding cycle. The negative vorticity that corresponds to clockwise rotation is shown by dashed lines while the positive vorticity that corresponds to anti-clockwise rotation is shown by solid lines. The negative and positive vortex grow from the top and bottom surface of the cylinder, respectively. At the

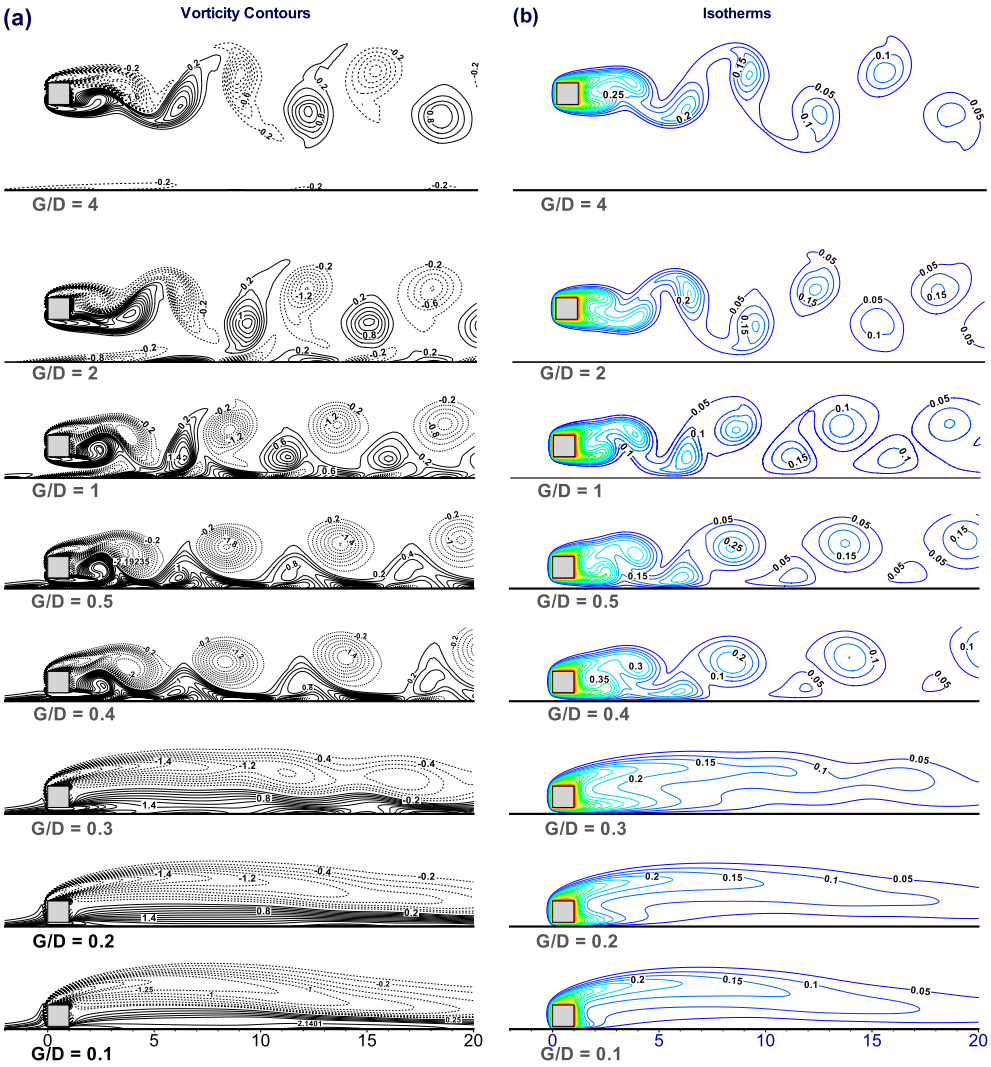

Fig. 4. Instantaneous contours of (a) vorticity (ω) and (b) isotherms at $Re = 100$ for various gap ratios, G/D, for the flow past a square cylinder near a plane moving wall. The isotherms are presented at the same instant of time for which the vorticity contours are drawn.

beginning of the cycle, lift is minimum and the drag is maximum (denoted by *A*). At this instant, the negative vortex is shed while the positive vortex grows and is continuously fed by the shear layer developing at the bottom surface. At *instant B*, the negative vorticity on the top surface continues to grow and starts to snap off the connection between the positive vorticity and the positive shear layer at the bottom surface of the cylinder. At *instant C*, the positive vortex is shed resulting in a maximum lift coefficient. The positive vortex grows and and starts to snap off the connection between the negative vorticity and the negative shear layer at the top surface of the cylinder at *instant D* and the process continues.

Contours of vorticity are presented at a smaller value of gap ratio i.e., $G/D = 1$ during a vortex shedding cycle along with the lift and drag coefficients as illustrated in Fig. 9(a) and (b). The scenario at this gap ratio is different from the case when $G/D = 4$. The drag coefficient has only one peak value during a cycle of vortex shedding and has the same frequency as that of the lift coefficient. At the beginning of the cycle (*instant A*), the negative vortex is shed while the positive vortex grows and is continuously fed by the positive shear layer developing at the bottom surface. At *instant B*, the negative shear layer formed along the wall, just below the bottom surface of the cylinder, aids in snapping off the supply for the positive vortex resulting in an early shedding of positive vortex at *instant B* itself rather than at instant C and the pair of vortices move downstream together. And thus the drag and lift coefficients have the same frequency. At *instant C*, the positive vortex is convected downstream along the moving wall while the negative vortex continues to grow.

Fig. 10(b) presents the scenario of vortex shedding at $G/D = 0.4$ during a cycle of shedding. The form of variation of drag and lift coefficient with time are similar to the case when $G/D = 1$ as seen in Fig. 10(*a*). At *instant A*, the negative vortex (top) is shed and the positive vortex grows (bottom) while it is being fed by the negative shear layer along the bottom surface of the cylinder. At *instant B*, the negative vortex from the top surface grows in size and constricts the positive vortex due to small gap. As a result the positive vortex is stretched, shed, and is convected along the wall at this instant. Both the negative and positive vortex move together downstream. The positive vortex is very weak compared to the negative vortex that is shed from the top surface. At *instant C*, the negative vortex continues to grow. The vortex shed from the top surface is near circular in shape, while the vortex shed from the bottom surface is substantially stretched in the flow direction similar to that observed at a higher Reynolds number of 500 in the work of Bhattacharyya and Maiti [17].

4.2. Distribution of pressure coefficient on the cylinder surface ($\overline{C}_P$)

The variation of time averaged pressure coefficient ($\overline{C}_P$) on the surface of the square cylinder is shown in Fig. 6 at different G/D. As seen in the figure, the pressure distribution strongly depends on the gap between the cylinder and the moving plane wall. The pressure coefficient shows a significant change along the bottom-half of the front face (AB) and at the bottom face (BC) of the cylinder with variation in G/D. Along the bottom face, the pressure coefficient is negative at $G/D = 4$ with a peak suction occurring at the upstream corner of the bottom surface. As the gap ratio is decreased the pressure coefficient increases enormously to higher positive values along this face. It should be noted that the difference between the pressure at the top and bottom surface of the cylinder results in a net lift force which contributes more to the total lift coefficient of the cylinder. As a result the average lift coefficient ($\overline{C}_L$) of the cylinder shoots up with decreasing G/D as evidenced from Fig. 5(a). Again, decreasing the gap ratio results in an increase in pressure coefficient along the bottom-half of the front face that results in a net increase in average drag coefficient

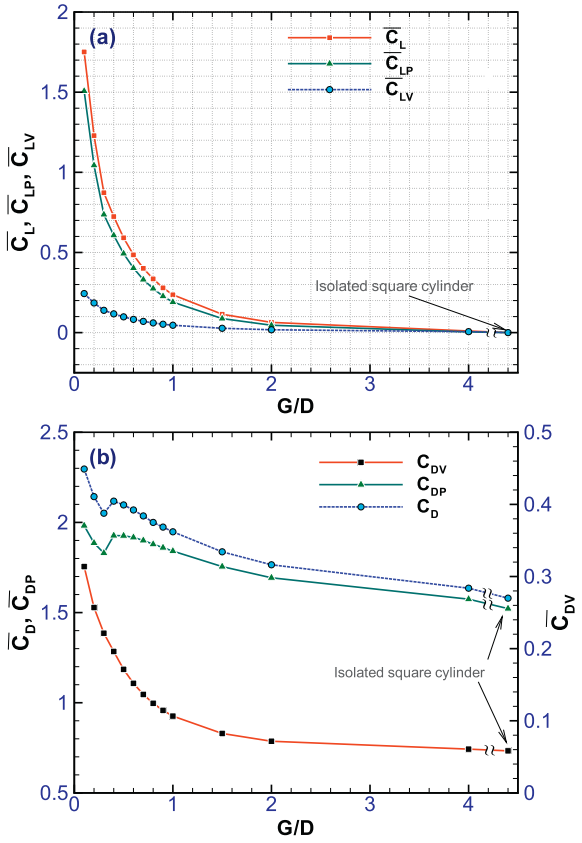

Fig. 5. Effect of gap ratio (G/D) on (a) Time averaged lift coefficient ($\overline{C}_L$), lift coefficient due to pressure and viscous forces ($\overline{C}_{LP}, \overline{C}_{LV}$) and (b) drag coefficient ($\overline{C}_D$), drag coefficient due to pressure and viscous forces ($\overline{C}_{DP}, \overline{C}_{DV}$) for the flow past a square cylinder near a moving wall.

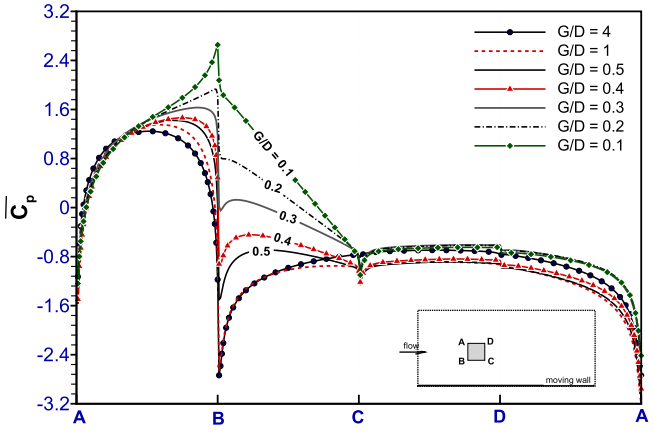

Fig. 6. Distribution of time averaged pressure coefficient ($\overline{C}_P$) on the surface of the square cylinder near a plane moving wall as a function of gap ratio, G/D.

($\overline{C}_D$) with decrease in gap ratio as seen in Fig. 5(b). Along the rear and top face, $\overline{C}_P$ diminishes when G/D is varied from 4 to 0.5 and starts to increase for $G/D \geqslant 0.4$.

4.3. Time averaged lift coefficient ($\overline{C}_L$)

The time averaged lift coefficient of the square cylinder along with the lift coefficient due to pressure and viscous forces are presented in Fig. 5(a) as a function of G/D. Looking at the figure, we observe that $\overline{C}_L$ is positive for all G/D. In general, $\overline{C}_L$ is close to zero

when $G/D = 4$ and rises rapidly to higher positive values with decreasing G/D. When the cylinder is far away from the moving wall, the lift coefficient oscillates with nearly the same positive maximum and negative minimum about zero and hence $\overline{C}_L$ is close to zero when $G/D = 4$. When the cylinder is brought closer and closer to the moving wall, the lift coefficient rises rapidly, mainly, due to changes in pressure distribution on the surface of the cylinder. Compared to lift coefficient due to viscous forces ($\overline{C}_{LV}$), the lift coefficient due to pressure forces ($\overline{C}_{LP}$) is greatly enhanced in the presence of a moving wall. Bhattacharyya and Maiti [17] observed a similar pattern of increasing lift coefficient with decrease in gap ratio from 0.5 to 0.1. for $Re < 600$.

4.4. Time averaged drag coefficient ($\overline{C}_D$)

The variation of time averaged drag coefficient ($\overline{C}_D$) of the cylinder as function of gap ratios is presented in Fig. 5(b). In general, there is a rise in drag coefficient with decrease in G/D. At $G/D = 4$, that is, when the cylinder is placed far away from the moving wall, the value of $\overline{C}_D$ is slightly higher than the case of an isolated square cylinder. Thus, it can be concluded that even at $G/D = 4$ the moving wall imparts a small drag force on the cylinder. When the cylinder approaches the moving wall (i.e., from $G/D = 4$ to 0.5), $\overline{C}_D$ rises gradually with increasing gap ratios as the moving wall imparts high pressure forces on the cylinder resulting in higher drag coefficients. At a critical gap ratio of 0.3, $\overline{C}_D$ drops and again rises with further decrease in gap ratio. This type of behaviour was also reported in the study of flow past a circular cylinder in the presence of a moving wall at different gap ratios by Yoon et al. [20] at $Re = 180$. A similar behaviour is observed for the drag coefficient due to pressure forces $\overline{C}_{DP}$. Unlike $\overline{C}_{DP}$, the drag coefficient due to viscous friction, $\overline{C}_{DV}$, is not affected at the critical gap ratio of 0.3. $\overline{C}_{DV}$ monotonously increases with decrement in gap ratio.

4.4.1. Strouhal number

The vortex shedding frequency of the square cylinder represented by the non-dimensional parameter called the Strouhal number, St, is presented in Fig. 7. The Strouhal number is calculated as per Eq. (12). At $G/D = 4$, the cylinder in the presence of a plane moving wall has a slightly higher Strouhal number compared to the isolated case and increases with decreasing gap ratio. For $4 \leqslant G/D \leqslant 1$, St increases linearly with G/D due to acceleration of flow in the gap between the cylinder and the moving wall due to decreasing gap ratio. When the cylinder is further brought close to the moving wall ($0.4 \leqslant G/D < 1$), St starts to decrease gradually as vortex shedding pattern is greatly altered i.e., two-rows of vortex shedding is transformed into single-row vortex shedding. Bhattcharyy and Maiti This can be realized from the vorticity contours presented in Fig. 4(a). For $G/D < 0.4$, Strouhal number does not appear due to suppression of vortex shedding. The three zones, namely, the twin-vortex shedding zone, single-row vortex shedding zone and the no-shedding zone are clearly indicated in the figure.

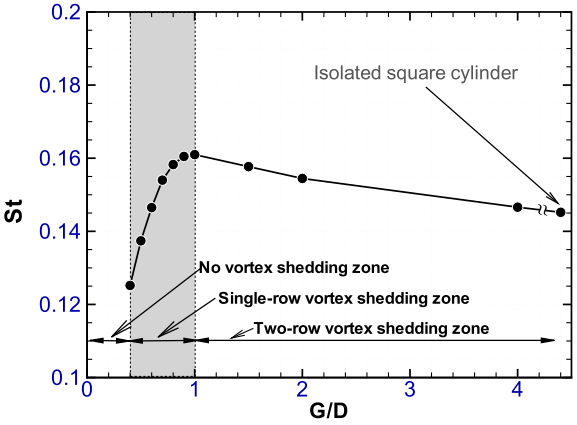

Fig. 7. Strouhal number (St) as a function of gap ratio (G/D) for the flow past a square cylinder near a moving wall.

4.4.2. Streamline pattern

Contours of streamlines for the flow past a square cylinder near a plane moving wall placed at gap ratios $0.1 \leqslant G/D \leqslant 4$ is depicted in Fig. 11(a). The streamlines presented here are time-averaged during a vortex shedding cycle (instantaneous for the steady flow, $G/D \leqslant 0.3$). A perfectly symmetric pattern is observed at $G/D = 4$ and 2. At $G/D = 1$, asymmetry sets in due to the modification of the flow in the presence of moving wall. The streamlines show an asymmetric pattern at $G/D = 0.5$. The quasi-steady nature of the flow is clearly evident at $G/D = 0.3$ and for $G/D < 0.3$, steady recirculating eddies are seen as vortex shedding is completely suppressed due to very small gap ratios between the cylinder and moving wall.

For the case of a isolated square cylinder, trailing edge separation occurs at $Re = 100$ [25]. Trailing edge separation is found to occur at the top surface for $G/D = 4$ and 2. With decreasing gap ratio (G/D), along the top surface, the flow separates at the leading edge and reattaches at a shorter distance close to the trailing edge. With further decrease in G/D, i.e., for $0.1 \leqslant G/D \leqslant 0.5$, the flow separates at the leading edge but does not reattach on the sides (of the top surface). At these gap ratios, the fluid from the wake enters the top surface of the cylinder as seen in Fig. 11(a) for $0.1 \leqslant G/D \leqslant 0.5$.

4.5. Heat transfer characteristics

4.5.1. Isotherms

Contours of instantaneous isotherms are presented in Fig. 4(b) at $G/D = 4$, 2, 1, 0.5, 0.3, 0.2 and 0.1 for the same instant at which the vorticity contours in the same figure (Fig. 4(a)) is drawn. When the cylinder is placed far away from the moving wall the isotherm pattern shows two rows of warm blobs being convected downstream the cylinder. When the cylinder is brought closer to the moving wall, the bottom row of warm blobs close to the moving wall are weak and are smaller in size compared to the top row (cf. Fig. 4 (b) at $G/D = 0.5$ and 0.4) and they move along the wall. At $G/D = 0.3$, the isotherms show a quasi-steady profile as the flow field becomes quasi-steady in nature due to suppression of vortex shedding. For $G/D \geqslant 0.2$, the isotherms show a steady pattern since vortex shedding from the cylinder is completely arrested.

The time-averaged isotherms show a symmetric pattern, along a line drawn through the centre of the cylinder parallel to the top and bottom surface, for $G/D = 4$ and 2 as shown in Fig. 11(b). For $G/D < 2$, the isotherms shown an asymmetric profile due to change in the flow pattern in the presence of moving wall. The boundary layer becomes very thin along the bottom surface of the cylinder, with decreasing gap ratios, resulting in higher heat transfer rates along this surface.

The form of isotherms during a vortex shedding cycle are shown in Figs. 8–10(c) at $G/D = 4$,1 and 0.4, respectively. As a passive scalar, the isotherms mimic the vorticity contours as seen in these figures. Heat from the cylinder surface is carried away, as warm blobs, by the vortices that are shed. At $G/D = 4$, the warm blobs emanating from the top and bottom surface are equal in size. With decrease in gap ratio, i.e., the at $G/D = 1$, the warm blobs emanating from the bottom surface are smaller in size. With further decrease in gap ratio ($G/D = 0.4$), the warm blobs emanating from the top and bottom surface are unequal is size and the one that is evolving from the bottom surface becomes smaller and is carried away by the moving wall.

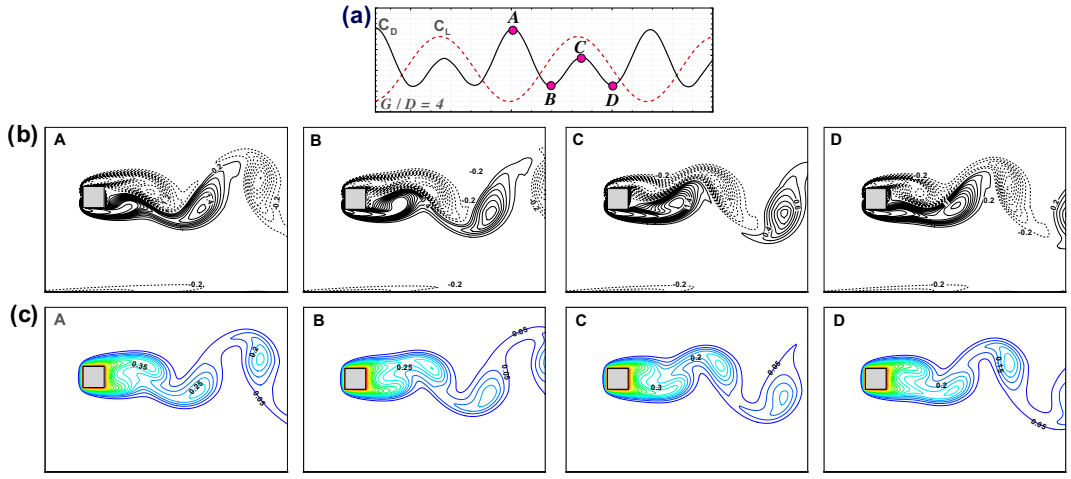

Fig. 8. (a) Time history of lift ($\overline{C}_L$) and drag ($\overline{C}_D$) coefficient during a vortex shedding cycle; (b) vorticity contours at different time instants of a vortex shedding cycle for the flow past a square cylinder placed at a gap ratio of $G/D = 4$ from a plane moving wall; (c) isotherms for the same instant of time for which the vorticity contours in (b) is presented.

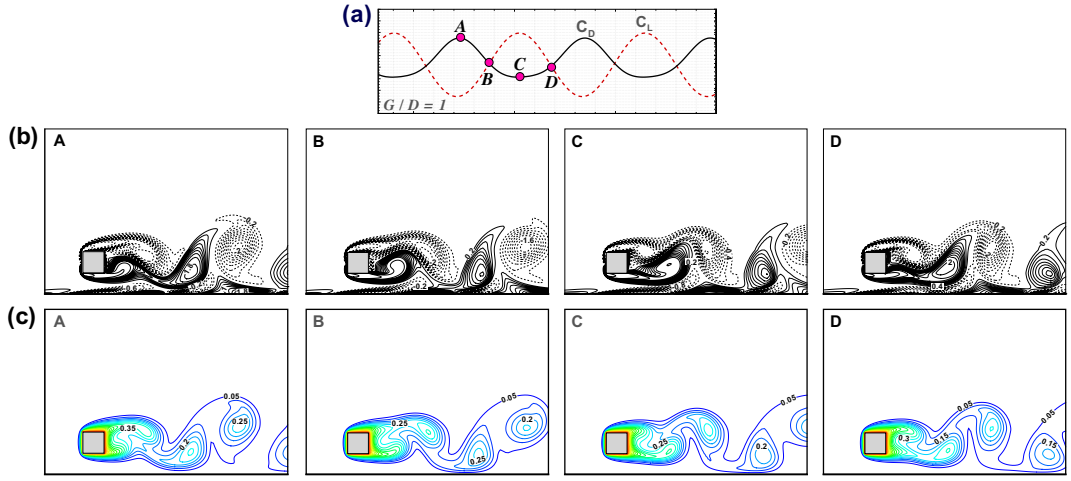

Fig. 9. (a) Time history of lift ($\overline{C}_L$) and drag ($\overline{C}_D$) coefficient during a vortex shedding cycle; (b) vorticity contours at different time instants of a vortex shedding cycle for the flow past a square cylinder placed at a gap ratio of $G/D = 1$ from a plane moving wall; (c) isotherms for the same instant of time for which the vorticity contours in (b) is presented.

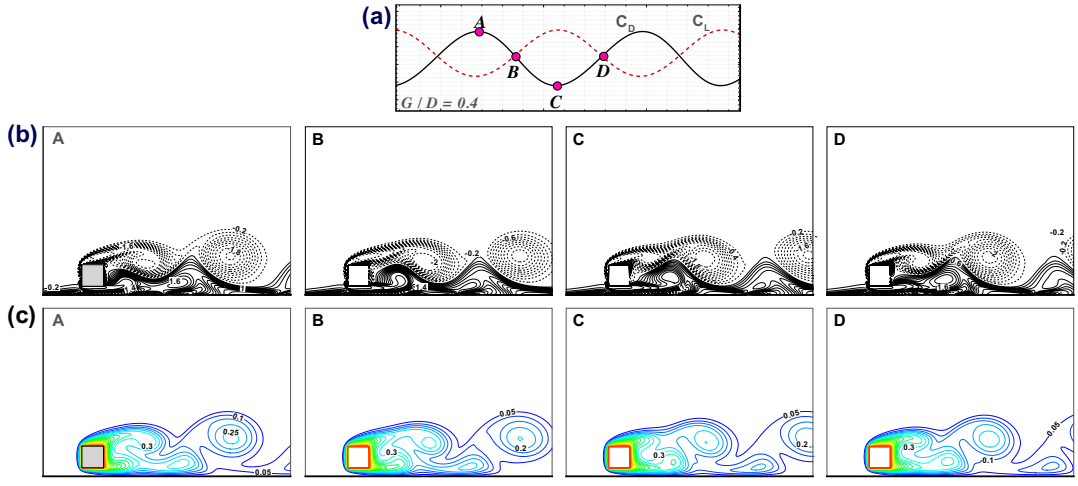

Fig. 10. (a) Time history of lift ($\overline{C}_L$) and drag ($\overline{C}_D$) coefficient during a vortex shedding cycle; (b) vorticity contours at different time instants of a vortex shedding cycle for the flow past a square cylinder placed at a gap ratio of $G/D = 0.4$ from a plane moving wall; (c) isotherms for the same instant of time for which the vorticity contours in (b) is presented.

4.5.2. Time evolution of mean Nusselt number (Nu_M) of the cylinder

Instantaneous variation of the time evolution of mean Nusselt (Nu_M) of the cylinder is presented in Fig. 12 as a function of non-dimensional time (τ) for different gap ratios. The profiles at $G/D = 4$, 2, 1, 0.5 and 0.4 shows that Nu_M oscillate periodically with time. When vortices are shed from the cylinder, heat is transported to the external fluid stream resulting in heat transfer augmentation that depends on gap ratio. At $G/D = 0.3$, the flow around the cylinder achieves a quasi-steady state and hence the thermal field, too, shows the same pattern resulting in an weakly oscillating Nu_M with time. When the cylinder is further placed close to the moving wall, the flow remains steady and as a result the thermal field, too, achieves a steady state that results in a steady profile of Nu_M with time at $G/D = 0.2$ as evident from the figure.

4.5.3. Local Nusselt number along the cylinder surface ($\overline{Nu}$)

The time averaged local Nusselt number ($\overline{Nu}$) along the surface of the cylinder is presented in Fig. 13(*a*) at $G/D = 4$, 1, 0.4, 0.3, 0.1

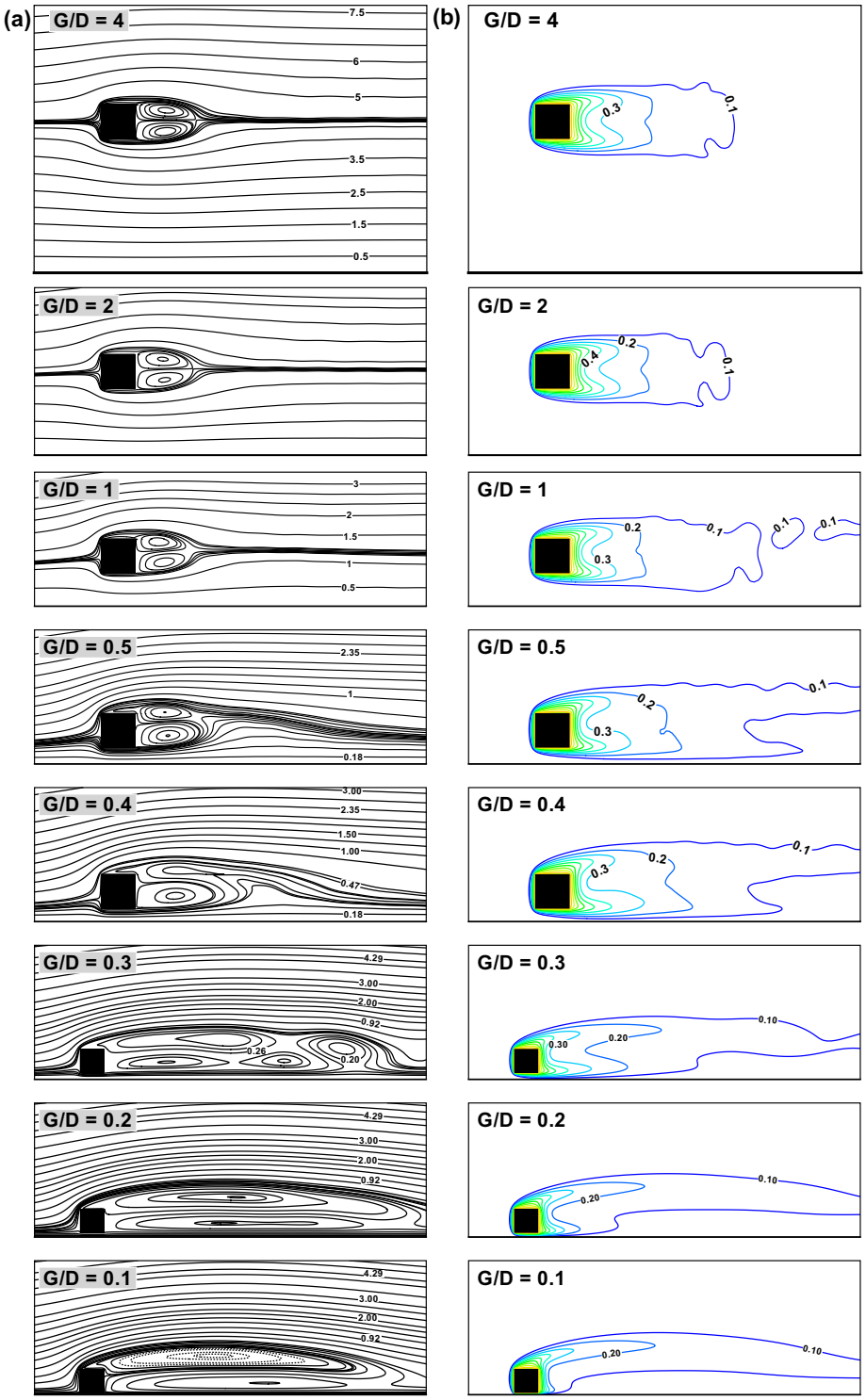

Fig. 11. Time-averaged (a) streamline and (b) isotherms patterns for the flow past a square cylinder placed at different gap ratio, G/D, from a plane moving wall.

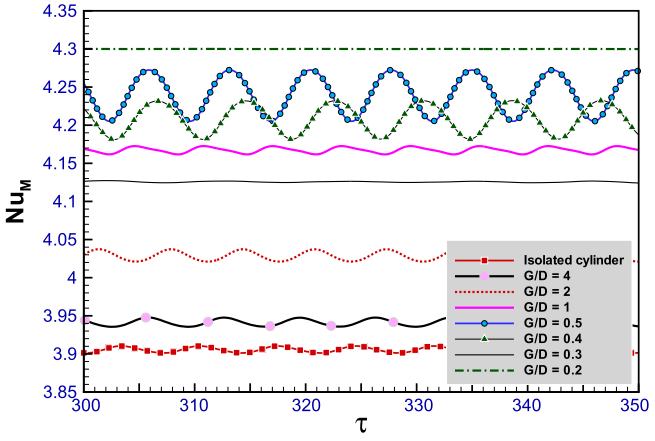

Fig. 12. Time evolution of mean Nusselt number (Nu_M) of the square cylinder at various gap ratios for the flow past a square cylinder near a plane moving wall.

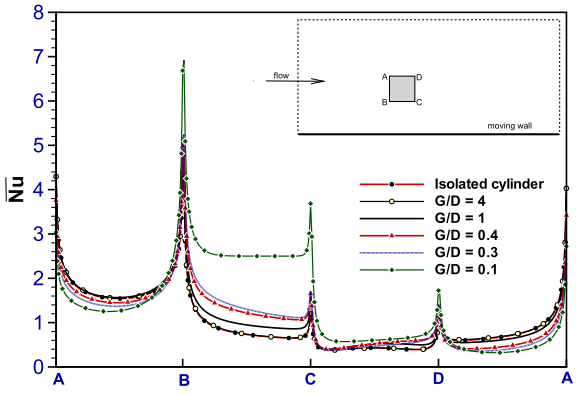

Fig. 13. Distribution of time-average local Nusselt (Nu) number along the surface of the square cylinder at various gap ratios, G/D.

and for the isolated case. Heat transfer along the faces seems to be strongly dependent on gap ratio. With a decrease in gap ratio, the local Nusselt number along the top-half of the front face (AB) decreases while it increases with decreasing gap ratio along the bottom-half of the same face. Along the bottom face (BC) of the cylinder, $\overline{Nu}$ increases with an increase in gap ratio. When the gap ratio decreases, the fluid flowing between the bottom surface of the cylinder and the moving wall carries away more heat resulting in high heat transfer rates. Along the bottom-half of the rear face (CD), there is no significant change in $\overline{Nu}$ for $0.1 \leqslant G/D \leqslant 4$ while it increases with decreasing gap ratio along the top-half of the rear face. The rear face has the highest heat transfer rate at $G/D = 0.1$ compared to any other gap ratio.

4.5.4. Average Nusselt number along the faces ($\overline{Nu}_{f,r,t,b}$)

The average Nusselt number along four different faces of the cylinder shows an interesting feature and is presented in Fig. 14(a) as a function of G/D. In general, for an isolated cylinder, the front face has high $\overline{Nu}$ while the rear face has the least value of $\overline{Nu}$ as shown in Fig. 14(a). The top and bottom surface have equal values. But for the case of a cylinder near a plane moving wall, the situation is different. Although the highest and lowest heat transfer rate occurs along the front and rear face, the top and bottom surface do not have the same heat transfer rates. The presence of moving wall aids in increasing the average Nusselt number and at the same time, it has a negative effect on the top

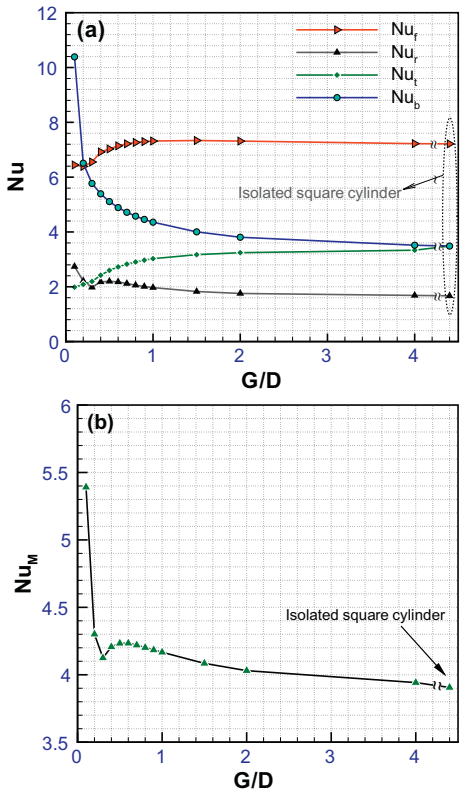

Fig. 14. (a) Average Nusselt number at the front (Nu_f), rear (Nu_r), top (Nu_t) and bottom (Nu_b) face of the square cylinder placed near a moving wall at $Re = 100$. (b) Mean Nusselt (Nu_M) of the square cylinder as a function of G/D.

surface. That is, the heat transfer along the top surface decreases with decrement in gap ratio.

Compared to the isolated case, $\overline{Nu}_f$ remains constant for $1 \leqslant G/D \leqslant 4$ and drops when G/D is reduced from 1 to 0.1. Along the bottom face, there is a gradual increase in $\overline{Nu}_b$ when $1 \leqslant G/D \leqslant 4$. For $G/D > 1$ it rises rapidly. It should be noted that at $G/D = 0.1$, the $\overline{Nu}_b$ surpasses the value of $\overline{Nu}_f$ at the same G/D. A gradual decrease in $\overline{Nu}_t$ is observed with decreasing gap ratio. The recirculating wake formed behind the cylinder enters the top surface and thus the thickness of thermal boundary layer formed along the top surface (cf. the streamlines and isotherms shown in Fig. 11(a) and (b) at $G/D = 0.1$) increases with decreasing G/D that eventually results in lower heat transfer rates along this face.

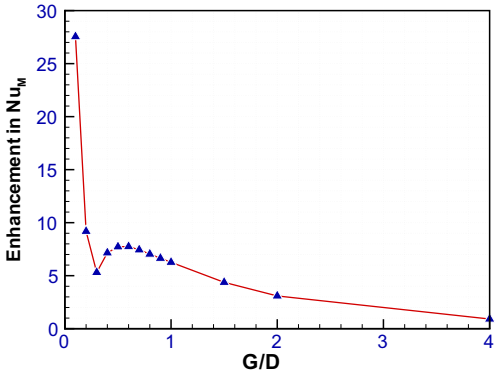

Fig. 15. Enhancement in mean Nusselt number of a square cylinder placed near a moving wall as a function of G/D.

4.5.5. Mean Nusselt number of the cylinder (Nu_M)

The effect of placing a cylinder at various gap ratios from a moving plane wall on the mean Nusselt number (Nu_M) of the cylinder, calculated as per Eq. (15), is shown in Fig. 14. In general, when an isolated cylinder is brought towards a moving wall, heat transfer enhancement occurs that depends on the gap between the cylinder and the plane moving wall. When the cylinder is sufficiently far away from the moving wall, the mean Nusselt number approaches the isolated case. For $0.5 \leqslant G/D \leqslant 4$, a linear increase in Nu_M observed. At $G/D = 0.4$, it starts to decline and dips at $G/D = 0.3$ to a low value (but higher than the case when $G/D = 1.5$) and it increases enormously when G/D is further decreased as shown in Fig. 14.

4.6. Enhancement in heat transfer

The enhancement in heat transfer or the percentage increase in heat transfer compared to the isolated case is presented in Fig. 15 as a function of G/D. By displacing the cylinder near a wall from $G/D = 4$ to 0.5 one can achieve a gradual increment in heat transfer rates. As much as 7.9% enhancement in heat transfer can be achieved at $G/D = 0.5$ by placing a cylinder near a plane moving wall compared to the case of an isolated cylinder. Placing the cylinder further close to the moving wall, but up to $G/D = 0.3$, diminishes the heat transfer rates. For example, at $G/D = 0.4$ the percentage increase in heat transfer rate is 7.25%. Whereas at $G/D = 0.3$, it further reduces to 5.3%. When the cylinder is placed too close to the moving wall, i.e., at $G/D = 0.2$ and 0.1, the percentage increase in heat transfer is enormous compared to the other cases with 9.25% and 27.45%, respectively.

5. Summary and Conclusions

A numerical study of flow and forced convection heat transfer from a square cylinder considering the effect of gap ratios (G/D) between the cylinder and a moving plane wall has been made for $0.1 \leqslant G/D \leqslant 4$ at $Re = 100$. The fluid is air and is moving with an uniform velocity. The plane wall is also moving with the same velocity as the uniform stream. Numerical simulation were performed using finite volume method based on SIMPLE algorithm. Some of the important conclusions from the study are presented as follows:

1. The flow is unsteady and periodic for $0.4 \leqslant G/D \leqslant 4$. Two-row vortex shedding is observed for $1 \leqslant G/D \leqslant 4$ while the flow is characterized by single-row of vortices for $0.4 \leqslant G/D < 1$. At $G/D = 0.3$, the flow is quasi-steady and for $G/D < 0.3$ vortex shedding is suppressed due to the presence of moving wall.
2. The average lift ($\overline{C}_L$) and drag coefficient ($\overline{C}_D$) of the cylinder increase with a decrement in gap ratio. The drag coefficient increases almost linearly with decrease in gap ratio and suddenly drop when the flow reaches a quasi-steady state at $G/D = 0.3$ and again starts to increase with decrement in gap ratio. For large gap ratios, these coefficients approach to their respective isolated cylinder case.
3. The average pressure coefficient ($\overline{C}_p$) along the bottom face and the bottom-half of the front face shows a significant change with decrease in gap ratio that results in an increase in the values of mean lift and drag coefficient. The Strouhal number (St) increases linearly with decrease in G/D from 4 to 1. With a further decrease in the gap ratio up to 0.4, it starts to reduce drastically due to alteration of the flow pattern in the presence of moving wall.
4. The average Nusselt number along the bottom surface ($\overline{Nu}_b$) of the cylinder rises gradually with decrement in gap ratio. Whereas, at the top face ($\overline{Nu}_t$) it diminishes with decrease in gap ratio. The average Nusselt number at the front face does not show any significant change for $1 \leqslant G/D \leqslant 4$ but reduces for $G/D < 1$. The study indicates that the presence of moving wall always results in augmentation of heat transfer from the cylinder compared to the isolated case. The augmentation is more prominent at gap ratios < 0.3. The obtained results indicate that as much as 27.45% increase in mean Nusselt number can be achieved, compared to the isolated case, by placing the cylinder at G/D=0.1.

Acknowledgement

I dedicate this paper to my beloved father M. Shanmugam (1948–2008) -S. Dhinakaran. The author thanks the anonymous reviewers for their constructive and valuable suggestion which helped in improving the quality of this paper.

References

[1] R. Blevins, Flow-induced vibration, Van Nostrand Reinhold Company, 1990.
[2] A. Okajima, Strouhal numbers of rectangular cylinders, J. Fluid. Mech. 123 (1982) 379–398.
[3] R.W. Davis, E.F. Moore, A numerical study of vortex shedding from rectangles, J. Fluid. Mech. 116 (1982) 475–506.
[4] S. Taneda, Experimental investigations of vortex streets, J. Phys. Soc. Jpn 20 (1965) 1714–1721.
[5] P.W. Bearman, M.M. Zdravkovich, Flow around a circular cylinder near a plane boundary, J. Fluid Mech. 89 (1978) 33–47.
[6] S.J. Price, D. Sumner, J.G. Smith, K. Leong, M.P. Paidoussis, Flow visualization around a circular cylinder near to a plane wall, J. Fluids Struct. 2 (2002) 175–191.
[7] S.C.C. Bailey, G.A. Kopp, R.J. Martinuzzi, Vortex shedding from a square cylinder near a wall, J. Turb. 3 (3) (2002) 1–18.
[8] S. Bhattacharyya, D.K. Maiti, Shear flow past a square cylinder near a wall, Int. J. Eng. Sci. 42 (2004) 2119–2134.
[9] N. Mahir, Three-dimensional flow around a square cylinder near a wall, Ocean Eng. 36 (2009) 357–367.
[10] Y. Yang, C. Chen, C. Chiu, Convective heat transfer from a circular cylinder under the effect of a solid plane wall, Int. J. Numer. Methods Fluids 23 (1996) 163–176.
[11] S.Z. Shuja, B.S. Yilbas, M.O. Budair, Vortex shedding over a rectangular cylinder with ground effect: flow and heat transfer characteristics, J. Eng. Math. 45 (2003) 309–334.
[12] S. Bhattacharyya, D.K. Maiti, S. Dhinakaran, Influence of buoyancy on vortex shedding and heat transfer from a square cylinder in proximity to a wall, Numer. Heat Transfer Part A 50 (2006) 585–606.
[13] D. Chakrabarty, R.K. Brahma, Effect of wall proximity in fluid flow and heat transfer from a rectangular prism placed inside a wind tunnel, Int. J. Heat Mass Transfer 51 (3-4) (2007) 736–746.
[14] A.K. Singha, A. Sarkar, P.K. De, Numerical study on heat transfer and fluid flow past a circular cylinder in the vicinity of a plane wall, Numer. Heat Transfer Part A 53 (2008) 661–666.
[15] M.P. Arnal, D. Georing, J.A.C. Humphrey, Vortex shedding from a bluff body adjacent to a plane sliding wall, J. Fluids Eng. 113 (1991) 384–398.
[16] S. Kumarasamy, J.B. Barlow, Computation of unsteady flow over a half-cylinder close to a moving wall, J. Wind Eng. Ind. Aerodyn. 69-71 (1997) 239–248.
[17] S. Bhattacharyya, D.K. Maiti, Vortex shedding from a square cylinder in presence of a moving wall, Int. J. Numer. Methods Fluids 48 (2005) 985–1000.
[18] W. Huang, H.J. Sung, Vortex shedding from a circular cylinder near a moving wall, J. Fluids Struct. 23 (7) (2007) 1064–1076.
[19] M.A. Jones, F.T. Smith, Fluid motion for car undertrays in ground effect, J. Eng. Math. 45 (2003) 309–334.
[20] H.S. Yoon, H.H. Chun, M.Y. Ha, H.G. Lee, A numerical study on the fluid flow and heat transfer around a circular cylinder near a moving wall, Int. J. Heat Mass Transfer 50 (2007) 3507–3520.
[21] H.S. Yoon, J.B. Lee, J.H. Seo, H.S. Park, Characteristics for flow and heat transfer around a circular cylinder near a moving wall in wide range of low Reynolds number, Int. J. Heat Mass Transfer 53 (23–24) (2010) 5111–5120.
[22] A. Sohankar, C. Norberg, L. Davidson, Low-Reynolds number flow around a square cylinder at incidence: study of blockage, onset of vortex shedding and outlet boundary condition, Int. J. Numer. Methods Fluids 26 (1998) 39–56.
[23] S.V. Patankar, Numerical heat transfer and fluid flow, Hemisphere Publishing Corporation, Taylor and Francis Group, New York, 1980.

[24] B.P. Leonard, A stable and accurate convective modeling procedure based on quadratic upstream interpolation, Comput. Meth. Appl. Mech. Eng. 19 (1979) 59–98.
[25] A. Sharma, V. Eswaran, Heat and fluid flow across a square cylinder in the two-dimensional laminar flow regime, Numer. Heat Transfer Part A 45 (2004) 247–269.
[26] Y. Shimizu, Y. Tanida, Fluid forced acting on cylinders of rectangular cross-section, J. Trans. Jpn. Soc. Mech. Eng. B 44 (1978) 2699–2706.
[27] R. Franke, W. Rodi, B. Schonung, Numerical calculation of laminar vortex shedding flow past cylinders, J. Wind Eng. Ind. Aerodyn. 35 (1990) 237–257.
[28] A. Sohankar, C. Norberg, L. Davidson, Numerical simulation of unsteady low-Reynolds number flow around rectangular cylinder at incidence, J. Wind Eng. Ind. Aerodyn. 69 (1997) 189–201.
[29] J. Robichaux, S. Balachandar, S.P. Vanka, Three-dimensional floquet instability of the wake of square cylinder, Phys. Fluids 11 (1999) 560–578.